Received: 25 September 2023 | Revised: 18 April 2024 | Accepted: 20 April 2024

DOI: 10.1002/nbm.5173

RESEARCH ARTICLE

NMR IN BIOMEDICINE WILEY

Navigator-based motion compensation for liver BOLD measurement with five-echo SAGE EPI and breath-hold task

Ke Zhang[1,2,3] | Simon M. F. Triphan[1,2,3] | Mark O. Wielpütz[1,2,3] | Christian H. Ziener[4] | Mark E. Ladd[5,6,7] | Heinz-Peter Schlemmer[4] | Hans-Ulrich Kauczor[1,2,3] | Oliver Sedlaczek[1,2,3,4] | Felix T. Kurz[4,8]

[1]Department of Diagnostic & Interventional Radiology, Heidelberg University Hospital, Heidelberg, Germany

[2]Translational Lung Research Center (TLRC), German Center for Lung Research (DZL), Heidelberg, Germany

[3]Department of Diagnostic & Interventional Radiology with Nuclear Medicine, Thoraxklinik at Heidelberg University Hospital, Heidelberg, Germany

[4]Division of Radiology, German Cancer Research Center, Heidelberg, Germany

[5]Division of Medical Physics in Radiology, German Cancer Research Center, Heidelberg, Germany

[6]Faculty of Physics and Astronomy, Heidelberg University, Heidelberg, Germany

[7]Faculty of Medicine, Heidelberg University, Heidelberg, Germany

[8]Division of Neuroradiology, Geneva University Hospitals, Geneva, Switzerland

Correspondence
Felix T. Kurz, Division of Radiology, German Cancer Research Center, 69120 Heidelberg, Germany.
Email: f.kurz@dkfz-heidelberg.de

Funding information
This work was supported by the Deutsche Forschungsgemeinschaft (DFG, German Research Foundation) (507778062) and by grants from the German Federal Ministry of Education and Research (BMBF) (82DZL004A1).

Purpose: The purpose of this work is to apply multi-echo spin- and gradient-echo (SAGE) echo-planar imaging (EPI) combined with a navigator-based (NAV) prospective motion compensation method for a quantitative liver blood oxygen level dependent (BOLD) measurement with a breath-hold (BH) task.

Methods: A five-echo SAGE sequence was developed to quantitatively measure T_2 and T_2^* to depict function with sufficient signal-to-noise ratio, spatial resolution and sensitivity to BOLD changes induced by the BH task. To account for respiratory motion, a navigator was employed in the form of a single gradient-echo projection readout, located at the diaphragm along the inferior–superior direction. Prior to each transverse imaging slice of the spin-echo EPI-based readouts, navigator acquisition and fat suppression were incorporated. Motion data was obtained from the navigator and transmitted back to the sequence, allowing real-time adjustments to slice positioning. Six healthy volunteers and three patients with liver carcinoma were included in this study. Quantitative T_2 and T_2^* were calculated at each time point of the BH task. Parameters of t value from first-level analysis using a general linear model and hepatovascular reactivity (HVR) of Echo1, T_2 and T_2^* were calculated.

Results: The motion caused by respiratory activity was successfully compensated using the navigator signal. The average changes of T_2 and T_2^* during breath-hold were about 1% and 0.7%, respectively. With the help of NAV prospective motion compensation whole liver t values could be obtained without motion artifacts. The quantified liver T_2 (34.7 ± 0.7 ms) and T_2^* (29 ± 1.2 ms) values agreed with values from literature. In healthy volunteers, the distribution of statistical t value and HVR was homogeneous throughout the whole liver. In patients with liver carcinoma, the distribution of t value and HVR was inhomogeneous due to metastases or therapy.

Abbreviations: BH, breath-hold; BOLD, blood oxygen level dependent; CVR, cerebrovascular reactivity; DCE, dynamic contrast enhanced; deoxy-Hb, deoxygenated hemoglobin; Echo1, first echo; EPI, echo-planar imaging; Et-CO_2, end-tidal CO_2; FB, free breathing; fMRI, functional MRI; FoV, field of view; GE/SE, gradient echo/spin echo; GLM, general linear model; HVR, hepatovascular reactivity; MGRE, multi-echo gradient echo; NAV, navigator based; PACE, prospective acquisition correction; ROI, region of interest; SAGE, spin and gradient echo; SPAIR, spectral attenuated inversion recovery; T_E, echo time; TOLD, tissue oxygen level dependent; T_R, repetition time.

Conclusions: This study demonstrates the feasibility of using a NAV prospective motion compensation technique in conjunction with five-echo SAGE EPI for the quantitative measurement of liver BOLD with a BH task.

KEYWORDS
hepatovascular reactivity, navigator-based slice tracking, prospective motion compensation, quantitative liver BOLD

1 | INTRODUCTION

Hypoxia is widely recognized as an unfavorable prognostic indicator for nearly all solid tumors and is also predictive of treatment failure across various therapeutic approaches, such as radiotherapy, chemotherapy, surgery, and targeted therapies.[1] The potential of imaging techniques to identify, map, and measure tumor hypoxia prior to treatment, as well as monitoring changes in hypoxia during therapy, is currently untapped in routine clinical practice. While positron emission tomography (PET)-based methods have been the main focus of hypoxia imaging research, emerging evidence suggests that MRI techniques may offer a practical and readily applicable alternative.[2]

Multiple functional MRI (fMRI) techniques, including blood oxygen level dependent (BOLD) MRI, tissue oxygen level dependent (TOLD) MRI, dynamic contrast-enhanced (DCE) MRI, and oxygen-enhanced (OE) MRI, have been developed to quantify changes in oxygen partial pressure (P_aO_2) within tumors.[2–4] MRI has been employed in the assessment of tumor hypoxia to predict treatment outcomes in both preclinical and clinical radiation studies.[5]

In BOLD MRI, deoxygenated hemoglobin (deoxy-Hb) serves as an endogenous contrast agent by increasing magnetic susceptibility and shortening the transverse relaxation time (T_2*) of water protons in surrounding tissues. Hypoxic tissues exhibit a higher proportion of deoxy-Hb, leading to a higher transverse relaxation rate ($R_2^* = 1/T_2^*$), which is expected to decrease during a hyperoxic respiratory challenge as deoxy-Hb becomes more saturated with oxygen. Studies conducted in rodents and humans have demonstrated an increase in the BOLD signal (corresponding to a decrease in R_2*) in various tumors, including hepatocellular carcinoma (HCC), and in response to breathing pure oxygen (100% O_2)[6–8] or a gas mixture containing high oxygen content (carbogen; 95% O_2 /5% CO_2 or 98% O_2/2% CO_2).[9–12] Since the saturation of hemoglobin with oxygen depends on arterial oxygen pressure and tissue oxygen partial pressure, R_2^* can be considered as an indicator of oxygenation.

However, quantitative BOLD measurements are affected by respiratory motion and are typically performed using a multi-echo gradient echo (MGRE) sequence with breath-holding before and after the gas challenge. It is worth noting that breath-holding triggers a BOLD response, leading to increased vascular CO_2 levels and thus vasodilation, thereby causing an elevation in T_2 and T_2^*. Moreover, the acquisition time required for a single MGRE measurement (15 s) is too long to capture real-time BOLD changes.

To overcome the issues associated with motion artifacts, a recently developed navigator-based (NAV) slice tracking technique has been integrated into a simultaneous gradient echo/spin echo (GE/SE) echo-planar imaging (EPI) sequence. This integration aims to compensate for respiratory motion in the imaging of kidney vascular architecture and arterial spin labeling.[13,14]

In this approach, a navigator signal was acquired using a gradient-echo projection readout through the diaphragm along the inferior–superior direction. The diaphragm position is calculated from the navigator signal, fed back to the sequence and used for real-time adjustment of slice position. The navigator acquisition can be inserted before each EPI excitation.

In this study, a navigator-based (NAV) five-echo spin- and gradient-echo (SAGE) EPI sequence was developed to quantitatively measure T_2 and T_2^* for the purpose of depicting microvascular dysfunction. The sequence is designed to provide adequate signal-to-noise ratio and spatial resolution, and sufficient sensitivity to BOLD changes achievable through breath-holding.

2 | METHODS

2.1 | Subjects and image acquisition

Six healthy volunteers (two female, four male, aged 33 ± 6 years) and three patients with liver carcinoma were examined prospectively using an 18-channel body and 16-channel spine receive RF coil on a 1.5 T scanner (MAGNETOM Aera, Siemens Healthineers, Erlangen, Germany). All participants provided written informed consent, and the study was approved by the institutional ethics committee.

All participants received a routine abdomen MRI protocol including a standard T_1-weighted sequence before and after administration of MRI contrast agent, a standard diffusion-weighted sequence, a standard T_2-weighted sequence, and a standard DCE MRI sequence.

Breath-hold (BH) respiratory challenges were integrated into the imaging protocol, as follows. For block-designed BH tasks, 110 measurements were obtained, which include five and a half BH/FB (free breathing) cycles with 20 measurements (32 s) per cycle and 10 measurements (16 s) per half cycle.

During these BH challenges, all participants received a NAV SAGE sequence (Figure 1). This sequence was constructed based on a combination of GE and SE-EPI sequences, incorporating five different echo times (T_E). The first two echoes were gradient-echo acquisitions, with T_E values of 8.46 and 19.27 ms, respectively. Subsequently, three mixed spin-echo acquisitions followed, with T_E values of 36, 47.19, and 58 ms. A navigator acquisition and fat suppression were inserted before each transverse imaging slice of the SAGE EPI sequence. The navigator signal was acquired using a gradient-echo projection readout through the diaphragm along the inferior–superior direction. Liver position information was calculated from this navigator signal, fed back into the sequence and used for real-time adjustment of the slice position. The detailed sequence parameters were as follows: field of view (FoV) = 400 mm × 240 mm, acquired resolution = 3.33 mm × 3.33 mm, slice thickness = 8 mm, slice number = 8, partial Fourier factor = 6/8, GRAPPA (Generalized Autocalibrating Partially Parallel Acquisitions) acceleration factor = 3, T_R = 1.6 s, inversion time for spectral attenuated inversion recovery (SPAIR) fat suppression = 90 ms, navigator FoV = 200 mm, navigator resolution = 64, navigator flip angle = 15°, navigator repetition time = 4.22 ms.

2.2 | Data processing

T_2 and T_2^* maps were calculated by using a multiparametric voxel-by-voxel fitting approach. For quantitative evaluations T_2 and T_2^* can be calculated as[15,16]

$$S(t) = \begin{cases} S_0\, e^{-tR_2^*} & t < \dfrac{T_{E,SE}}{2} \\ {}^{S_0}/_{\delta}\, e^{-T_{E,SE}\left(R_2^* - R_2\right)}\, e^{-t\left(2R_2 - R_2^*\right)} & t > \dfrac{T_{E,SE}}{2} \end{cases} \quad (1)$$

where $S(t)$ is signal acquired at different echo time t, S_0 is the signal at $t = 0$, $R_2 = 1/T_2$ and $R_2^* = 1/T_2^*$. $T_{E,SE}$ is the echo time for Echo 5. The additional parameter δ is needed[17] to account for signal difference owing to imperfectly matched slice profiles between echo trains acquired before and after the refocusing pulse. Four parameters, R_2, R_2^*, S_0 and δ, were determined from a single multi-parametric fit. A representative fit is shown later in Figure 4.

2.3 | Statistical analyses

Statistical analyses were performed to create images that reveal regions exhibiting significant signal changes in response to the BH task. The first-level analysis of the first echo signal (Echo1), T_2 and T_2^* time series was performed for each subject using SPM12 (Wellcome Trust Centre for

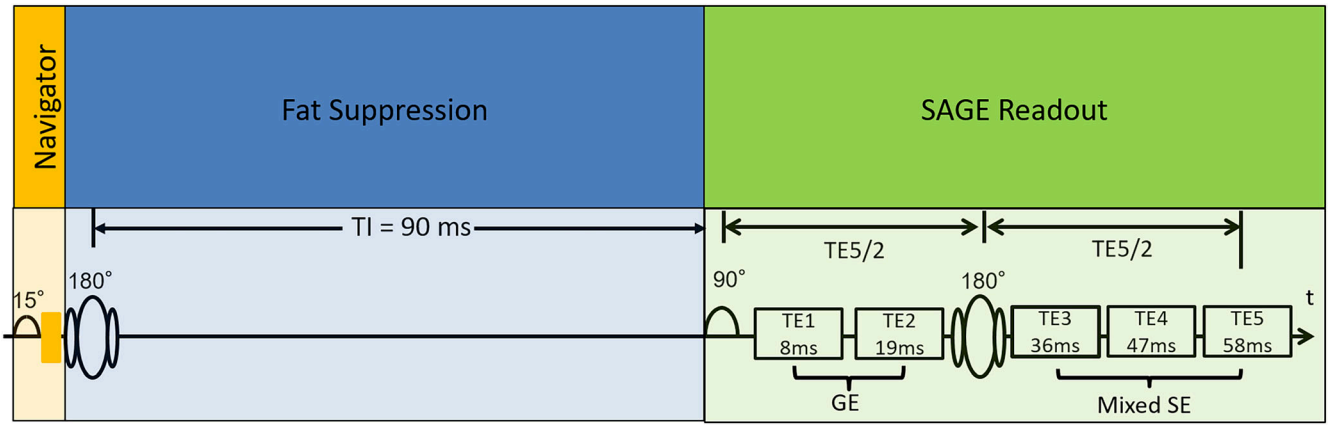

FIGURE 1 The sequence diagram of the five-echo SAGE technique is illustrated. This sequence is constructed based on a combination of gradient-echo (GE) and spin-echo (SE) EPI sequences, incorporating five different T_E values. The first two echoes are gradient-echo acquisitions, with T_E values of 8 and 19 ms, respectively. Subsequently, three mixed spin-echo acquisitions follow, with T_E values of 36, 47, and 58 ms. A navigator acquisition and fat suppression are included before each transverse imaging slice of the SAGE EPI sequence.

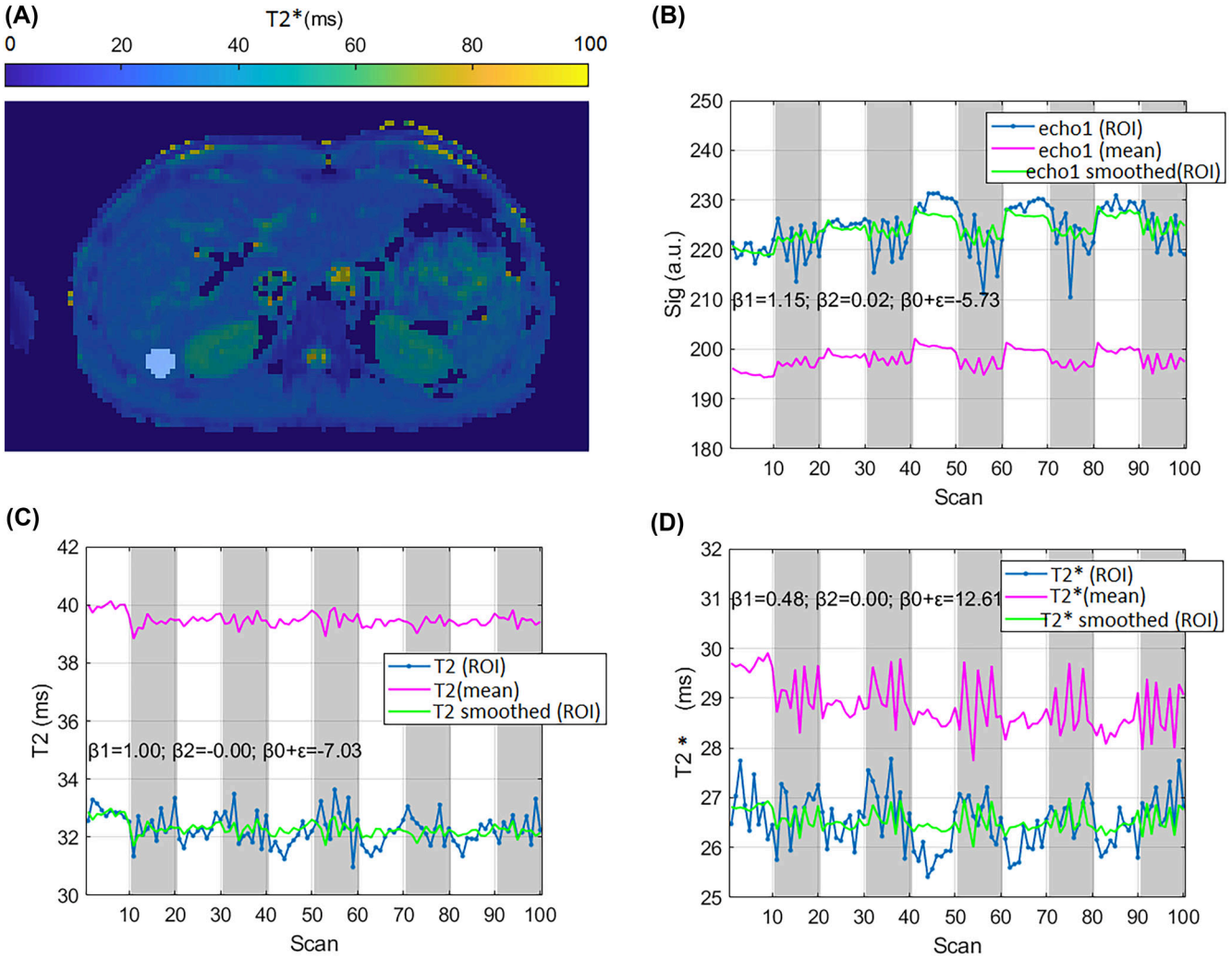

FIGURE 2 A, An elliptical ROI was chosen by utilizing a T_2^* map in Subject 2. B, The estimation of β coefficients of Echo1 within the selected ROI. Gray shading indicates periods of FB. C, The estimation of β coefficients of T_2 time series within the selected ROI. D, The estimation of β coefficients of T_2^* time series. The signal of the selected light blue region is blue, the mean signal of the entire liver used for fitting is pink and the fitted signal is plotted as a green line. The smoothed signals are Equation 3 fitted to show the time curve, giving an estimation of β_{0-2}.

Neuroimaging, UK) implemented in MATLAB 2021a (MathWorks, Natick, MA, USA). The initial 10 time points during the first half FB cycle were excluded from this analysis for subject adaptions. *t* values were calculated from first-level analysis using a general linear model (GLM). This analysis was performed for Echo1, T_2 and T_2^*. The general formula for the *t* value in the context of a GLM is as follows:

$$t = \frac{\widehat{\beta}_j}{\sqrt{\mathrm{Var}\left(\widehat{\beta}_j\right)}}. \tag{2}$$

$\widehat{\beta}_j$ is the estimated parameter for the *j*th contrast. This parameter represents the effect size or regression coefficient associated with the condition or contrast of interest. Var($\widehat{\beta}_j$) is the estimated variance of $\widehat{\beta}_j$. This represents the uncertainty or variability associated with the estimated parameter.

2.3.1 Hepatovascular reactivity analyses

Similar to calculation of a cerebrovascular reactivity (CVR) map, we performed voxel-wise calculation of hepatovascular reactivity (HVR).

In traditional CVR analysis, measurements of end-tidal CO_2 (Et-CO_2) are required and used in this linear regression equation[18]:

$$\text{dynamic MRI} = \beta_1\,\text{EtCO}_2 + \beta_2 t + \beta_0 + \varepsilon, \tag{3}$$

where β_1, β_2, and β_0 are estimated coefficients. t is the time index along the task acquisition. The term $\beta_2 t$ is included to account for any linear drift in the dynamic MRI values, and ε denotes the residual error. This linear regression analysis was performed for all BF and FB values. HVR, expressed as a percentage change in signal per mmHg of Et-CO_2 change, is calculated as

$$\text{HVR} = \frac{\beta_1}{\beta_1\,\min(\text{EtCO}_2) + \beta_0} \tag{4}$$

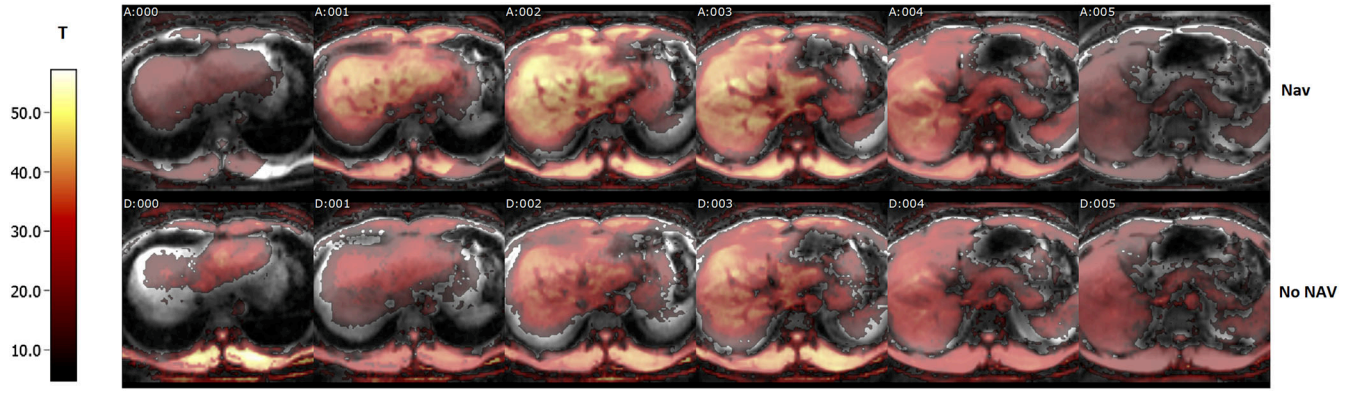

FIGURE 3 Comparison of the t values based on Echo1 after first-level analysis before and after using NAV motion compensation. One can observe differences between the T maps and the EPI images at the top slices without NAV. t values in the liver region were generally higher than those without NAV.

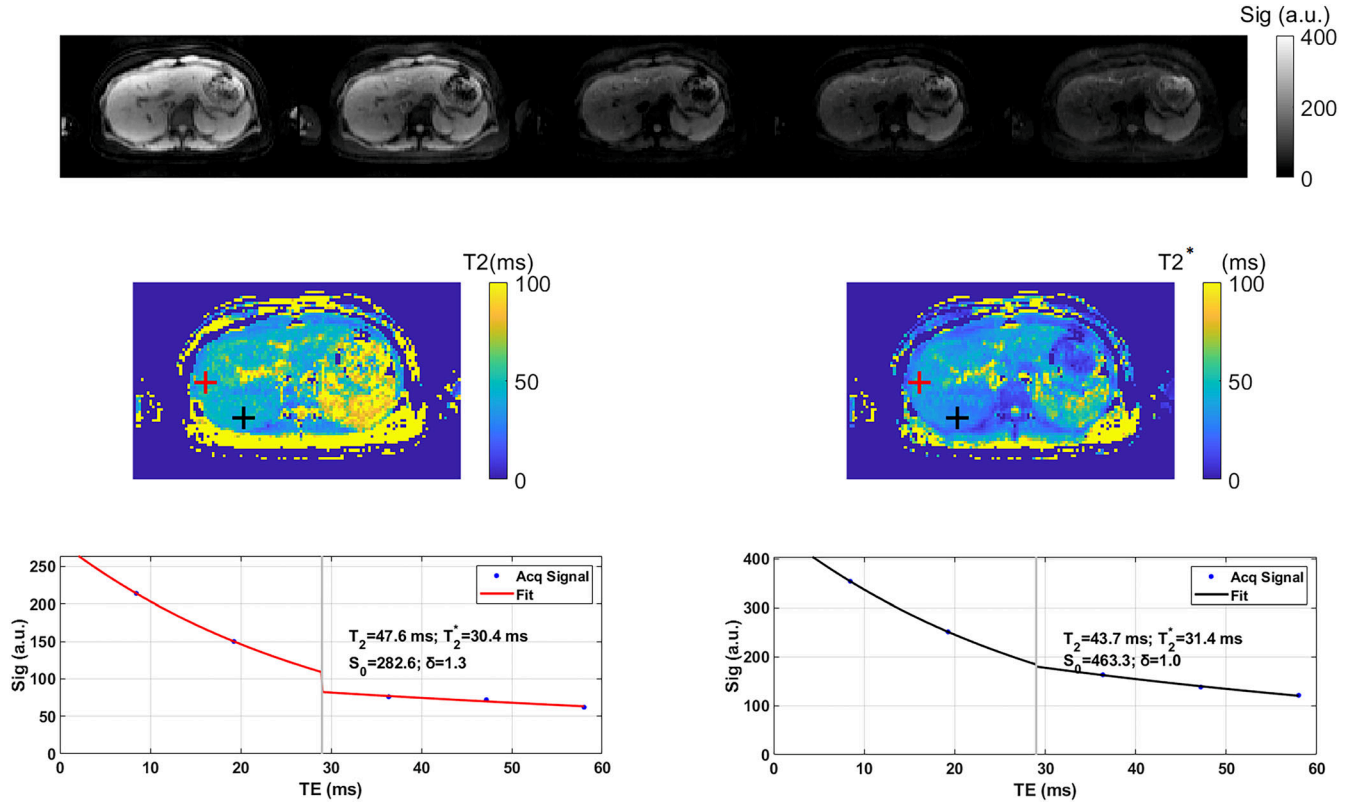

FIGURE 4 Five echoes generated from the SAGE sequence (first row). The quantified liver T_2 (34.7 ± 0.7 ms) and T_2^* (29 ± 1.2 ms) values were measured at the first time point of the BOLD task (second row). Nonlinear least-square fitting was performed for two representative voxels.

Without the measurement of Et-CO_2, the HVR was computed by replacing Et-CO_2 with the mean signal in our case. Relative HVR (rHVR) was computed as the HVR divided by the mean HVR in the liver region.[19]

3 | RESULTS

Figure 2 shows how the β values are evaluated. A spherical region of interest (ROI) was delineated at the liver. The mean curves of Echo1, T_2 and T_2^* from this example ROI are shown. Figure S1 shows the BOLD signals of Echo1, T_2 and T_2^* from a tumor ROI and liver ROI. During the 16 s BH task, the T_2^*-weighted signal from Echo1 was decreased; however, an increase in quantitative T_2 and T_2^* values could be found during the same period.

Using the NAV prospective motion compensation, motion artifacts were mitigated, allowing for the acquisition of a motion artifact-free whole liver t value (Figure 3). The t value derived from the first-level analysis of Echo1 indicated that the top portion of the liver was not captured without NAV prospective motion compensation. We also observed mismatches between the T map and the EPI images. Conversely, with the assistance of NAV, no motion artifacts were observed, and the t values in the liver region exhibited higher values than without NAV.

A five-echo measurement was performed using the SAGE sequence, as demonstrated by the high-quality and fat-suppressed images in Figure 4. Nonlinear least-square fitting was applied to each voxel, yielding T_2 values of 47.6 and 43.7 ms and T_2^* values of 30.4 and 31.4 ms in two representative voxels. Mean liver T_2 (34.9 ± 0.3 ms) and T_2^* (25.9 ± 0.2 ms) values were quantified after fitting and then averaging over

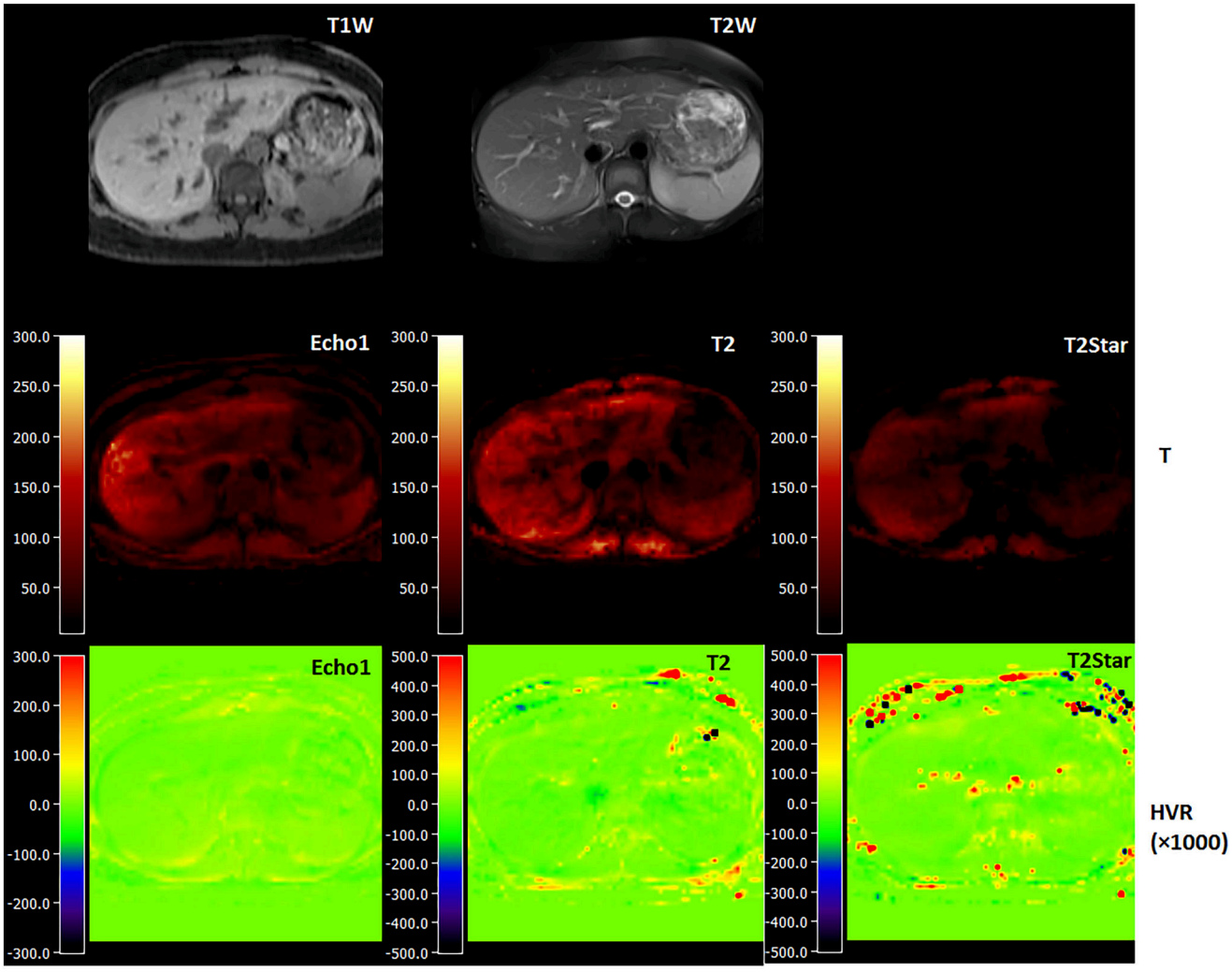

FIGURE 5 t value (second row) and HVR (third row) were calculated based on Echo1, T_2 and T_2^* time series.

the entire liver in this representative subject during the BH period. Mean liver T_2 (34.6 ± 0.4 ms) and T_2^* (25.7 ± 0.4 ms) values were found during the FB period *t* values, and HVRs were calculated based on Echo1, T_2 and T_2^* time series.

In a healthy volunteer, the distribution of statistical *t* values and HVR exhibited homogeneity throughout the entire liver, with identifiable vessel structures in the *t* values (Figure 5).

In patients with liver carcinoma, the distribution of *t* values and HVR was altered compared with a healthy volunteer (Figure 5) due to metastases or therapy, as depicted in Figures 6–8. In the first patient (69 years, male, liver metastasis of colon carcinoma), shown in Figure 6, a ring surrounding the tumor could be discerned in the *t* values. This ring exhibited higher *t* values and coincided with the metastasis identified in T_2-weighted images. Inside the ring, the *t* values were lower. However, HVR, particularly T_2-based HVR and T_2^*-based HVR, demonstrated higher values within the ring.

In the second patient (76 years, male, liver metastasis of colon carcinoma), the contrast-enhanced T_1-weighted images revealed an enhanced region within the liver (Figure 7). However, there were no discernible changes in the *t* values, T_2-based HVR or T_2^*-based HVR. The Echo1-based HVR exhibited a relatively low value in this region. In the third patient (77 years, male, liver metastasis of colon carcinoma), the ADC map and T_2-weighted images depicted an enhanced region in the liver (Figure 8). The highlighted region demonstrated a decrease in all three types of *t* value. Additionally, the three types of HVR in this region showed decreased values, with T_2-based HVR and T_2^*-based HVR even exhibiting negative values.

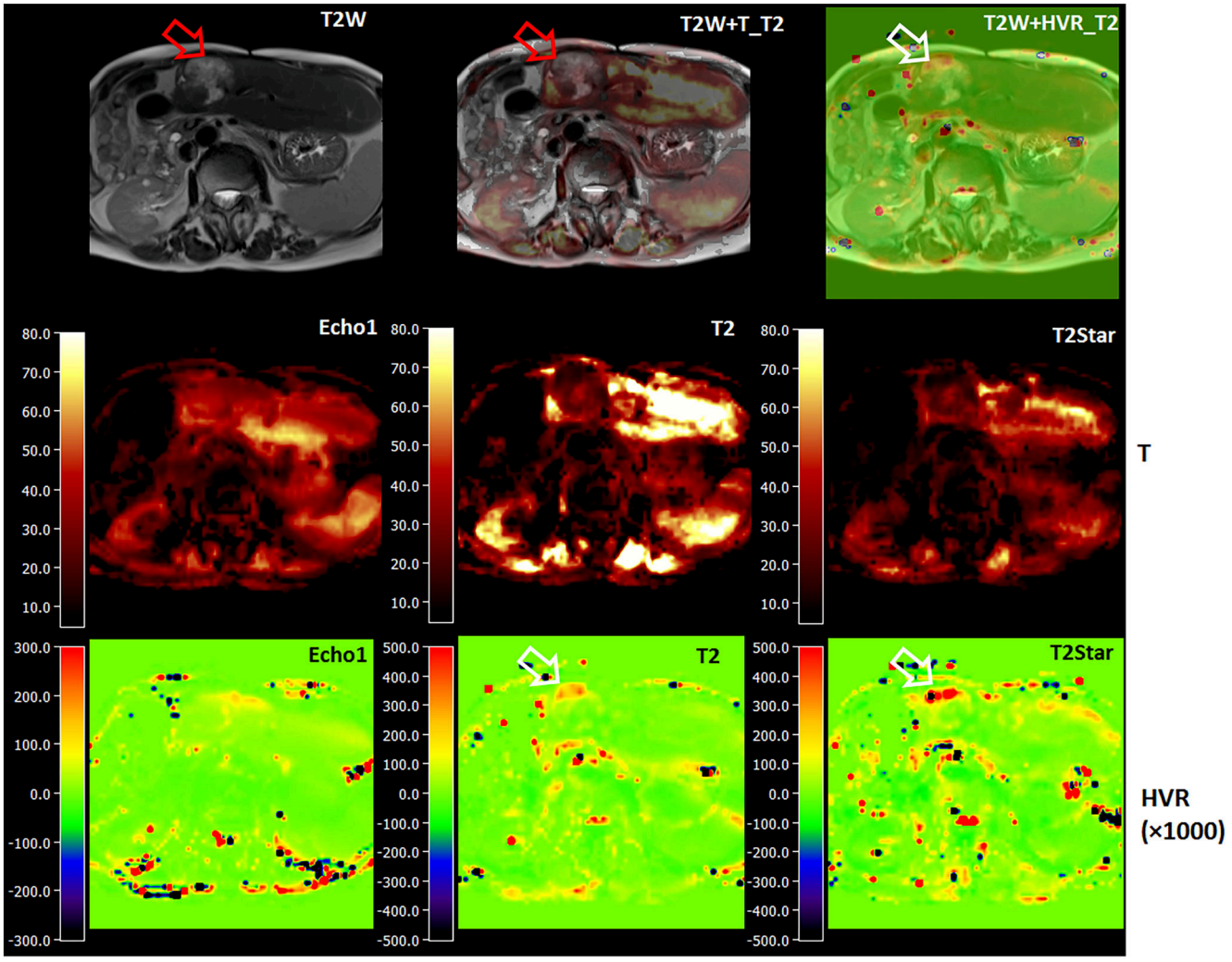

FIGURE 6 Anatomical and BOLD results for the first patient (69 years, male, liver metastasis of colon carcinoma). The top row displays a T_2-weighted image with overlays of T_2-based *t* values and T_2-based HVR. The middle row represents the *t* values computed using different contrasts, namely, Echo1, T_2 and T_2^* time series. The bottom row shows HVR values (multiplied by 1000) calculated based on Echo1, T_2 and T_2^* time series. *t* exhibits higher values at the outer periphery of the tumor but lower values within the tumor. In contrast, T_2-based HVR and T_2^*-based HVR demonstrate enhanced values within the tumor region (arrows).

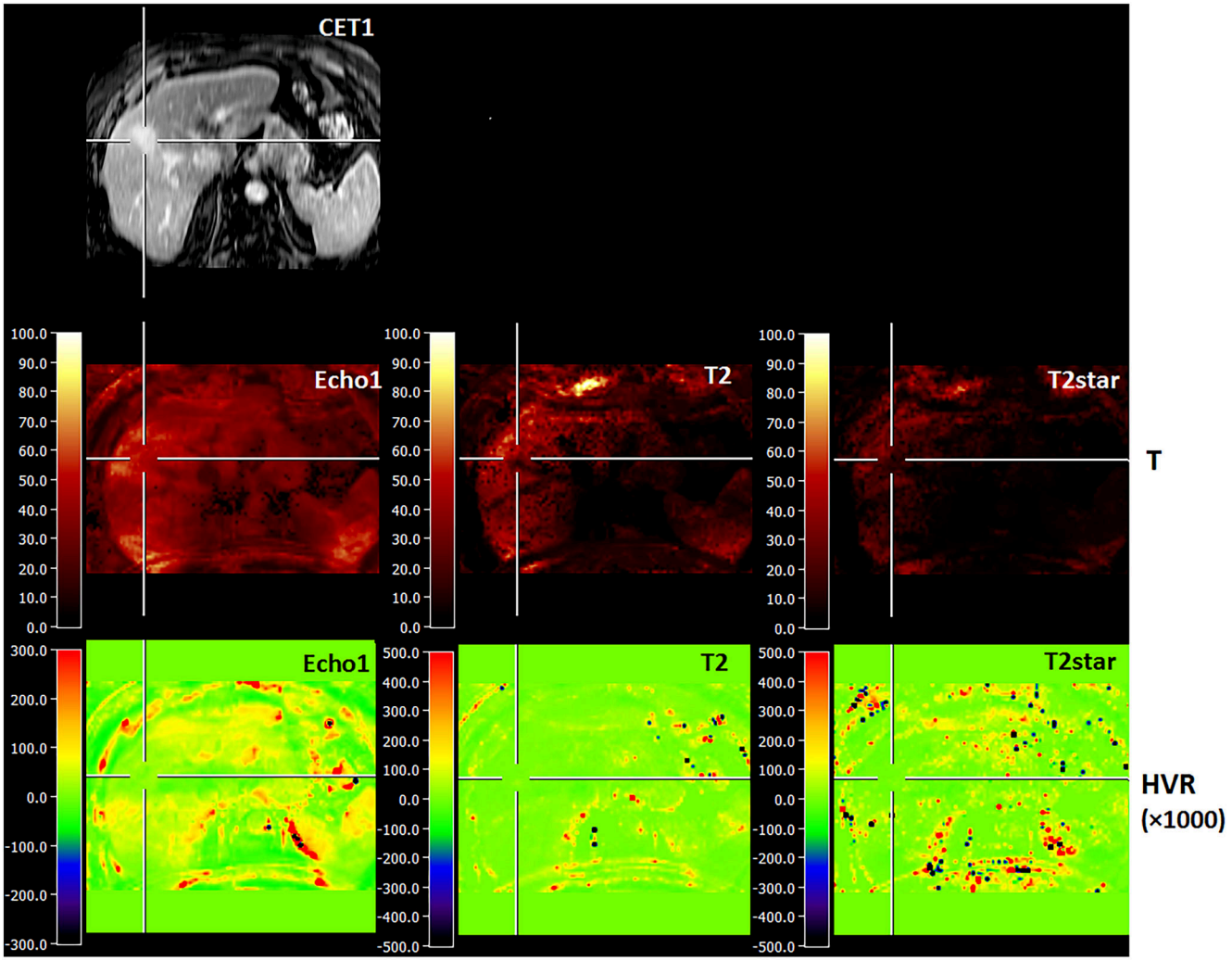

FIGURE 7 Anatomical and BOLD results for the second patient (76 years, male, liver metastasis of colon carcinoma). The first row is a contrast-enhanced T_1-weighted image, which shows an enhanced region. The second row is *t* values calculated based on the Echo1, T_2 and T_2^* time series. The third row is HVR (multiplied by 1000) calculated using Echo1, T_2 and T_2^* time series. Echo1-based HVR shows a relatively low value in this region.

4 | DISCUSSION

In this study, a five-echo SAGE sequence was developed to quantitatively measure T_2 and T_2^* for the assessment of microvascular dysfunction and BOLD changes during the BH task. To address respiratory motion, a navigator was utilized as a single gradient-echo projection readout located at the diaphragm along the inferior–superior direction. The developed NAV SAGE technique effectively compensated for respiratory motion in real time.

The rationale for selecting BH as the task is its relative ease of implementation when compared with hypercapnia and hypoxia, which require additional masks and devices for monitoring CO_2 and O_2 concentrations.

Considering the challenges faced by elderly patients, the BH task was limited to a duration of only 16 s for BOLD measurement. During this BH period, the concentration of deoxy-Hb in the blood, which is paramagnetic, increased. As a result, the T_2^*-weighted signal should be decreased while T_2 and T_2^* decreased. BH tasks with longer duration could be used and might induce vasodilation, which would lead to the opposite changes in T_2 and T_2^*. Nonetheless, for the majority of patients examined here, 16 s represented the longest possible BH duration. The advantage of quantitative liver BOLD can also be observed in the signal trend of Echo1, T_2 and T_2^* in Figure 2: several possible influences could affect the signal, such as spin inflow, T_1- or B_1-related effects. For instance, the opposite behavior of Echo1 compared with that of quantitative T_2 and T_2^* could be explained by an inflow effect.

Usually, the acquisition time required for a single MGRE measurement (15 s) is too long to capture real-time BOLD changes; the SAGE sequence in this study, however, which measures quantitative T_2 and T_2^* with a T_R of 1.6 s, solves this problem. Another benefit of the proposed

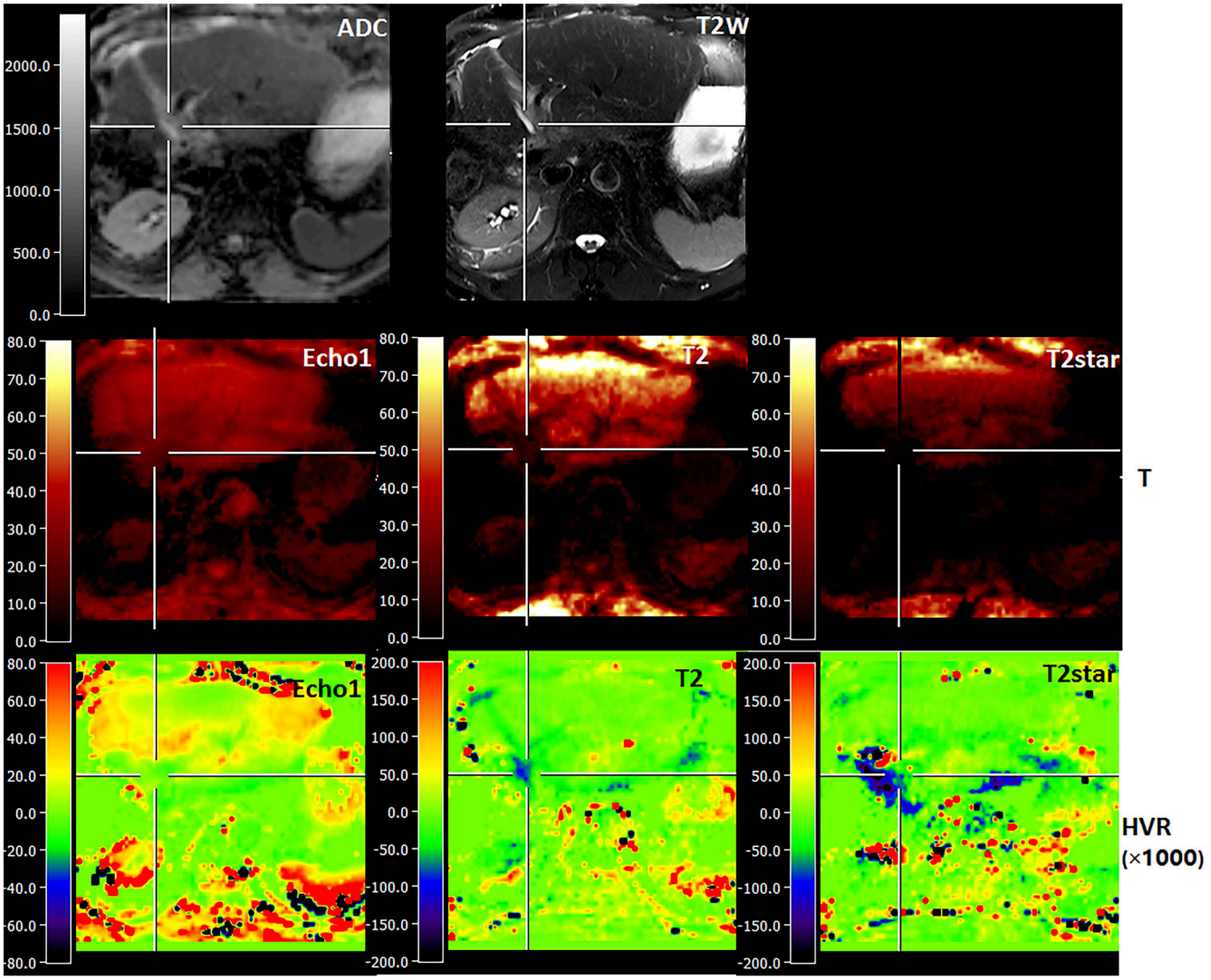

FIGURE 8 Anatomical and BOLD results for the third patient (77 years, male, liver metastasis of colon carcinoma). The top row comprises an ADC map and a T_2-weighted image, both indicating the presence of an enhanced region. The middle row displays t values computed from Echo1, T_2 and T_2^* time series. The bottom row shows HVR values (multiplied by 1000) derived from Echo1, T_2 and T_2^* time series. All three types of t value demonstrate a decrease in the highlighted region, while the corresponding HVR values show a relative decrease. Notably, T_2-based HVR and T_2^*-based HVR even exhibit negative values within this region.

sequence is that it provides T_2 and T_2^* maps simultaneously as opposed to only T_2^*. Having two contrasts helps us to understand more about their interplay and dynamic changes. Oxygen extraction function (OEF)[20] and venous vessel size[21] could be calculated in further studies.

Comparison with the non-NAV approach revealed that the NAV method reduced motion artifacts, particularly at the top of the liver, and resulted in higher t values throughout the liver (Figure 3). These results demonstrate the advantages of our NAV prospective motion compensation technique. Without the NAV technique, image registration or realignment would be necessary prior to BOLD analysis, which is challenging for liver images based on the EPI sequence.

The quantified liver T_2 values (34.7 ± 0.7 ms) and T_2^* values (29 ± 1.2 ms) obtained from Figure 4 are consistent with values reported in the literature.[22,23] As reported in a previous study,[23] the normal range for global T_2 values was 35–54 ms in males and 39–54 ms in females. The averaged T_2^* in healthy liver at 1.5 T was 28.5–33.3 ms in one study[22] and was about 21–35.2 ms in another.[24] In healthy subjects, the distribution of statistical t values and HVR appears homogeneous throughout the entire liver (Figure 5). However, in patients with liver carcinoma, the distribution of t values and HVR is altered due to the presence of metastases or the effects of therapy (Figures 6–8).

The observed increase in HVR within the tumor in Figure 6 indicates an elevation in microvasculature, possibly due to the presence of new metastases. The presence of this ring might be attributed to the tumor exerting pressure on the surrounding tissue. Conversely, the decrease in HVR observed in Patients 2 and 3 may be attributed to hypoxia or necrosis resulting from radiotherapy or chemotherapy. To find the correlation of HVR with tumor properties more patients need to be measured and studied. Pathological confirmation needs to be performed in future studies.

There are multiple limitations to this study. First, we only compensated for motion along the inferior–superior direction of the diaphragm using a one-dimensional navigator. To address motion along the anterior–posterior direction, an additional navigator could be employed, but this would extend the measurement and reconstruction time accordingly. Nevertheless, the existing method proved adequate in ensuring stable signals during the contrast agent pass-through. Second, the BH task with 16 s BH duration provided less BOLD SNR compared with hypercapnia and hypoxia approaches. Furthermore, no additional echoes were gathered beyond the spin-echo peak. If this had been implemented, it might have allowed for the calculation of parameters using only the refocusing echo, thus eliminating the need for slice correction with δ.[25]

BOLD-fMRI has a relatively long scanning time. Motion compensation is thus very important to enhance the statistical significance of the activation maps. Currently, retrospective motion correction techniques are widely adopted and integrated into various fMRI analysis toolboxes. Usually, retrospective volume-by-volume image registration is performed to eliminate motion effects. These methods offer advantages such as robustness, independence from sequence specifics and minimal disruption to the fMRI study setup. However, they fall short in delivering precise intra-volume correction and cannot address spin-history effects. On the other hand, the implementation of prospective motion correction in fMRI has demonstrated effectiveness in reducing false positives and enhancing sensitivity compared with retrospective techniques, especially in instances of significant motion.[26] Among prospective motion correction methods, NAV,[27] optical tracking[26] and the prospective acquisition correction (PACE) framework[28] have been employed in brain fMRI. Due to the internal respiratory motion in liver fMRI, optical tracking is not practical. Within the PACE framework, every 3D volume underwent registration directly to the reference image at the scanner as soon as the data became accessible. Subsequently, the registration information was relayed back to the sequence control unit to facilitate the updating of scanning parameters. Due to the long reconstruction and registration time, inter-volume delays need to be considered.

This study demonstrates the potential of the SAGE technique in combination with NAV prospective motion compensation for the quantitative assessment of liver BOLD. Simple BH tasks were performed without the measurement of Et-CO_2 to assess HVR. In future studies, respiratory tasks such as hypercapnia (5% CO_2) and hypoxia (100% O_2) can be incorporated. To calculate quantitative HVR, simultaneous measurement of Et-CO_2 is required. The acquisition of B_0 and B_1 maps could also be included to investigate the effects of field inhomogeneities on this technique.

5 | CONCLUSION

In conclusion, this study establishes the feasibility of utilizing quantitative liver BOLD in conjunction with a NAV prospective motion compensation technique during respiratory challenge.

CONFLICT OF INTEREST STATEMENT

The authors declare that they have no known competing financial interests or personal relationships that could have appeared to influence the work reported in this paper.

ACKNOWLEDGEMENTS

Open Access funding enabled and organized by Projekt DEAL.

DATA AVAILABILITY STATEMENT

The data that support the findings of this study are available from the corresponding author upon reasonable request.

REFERENCES

1. Hompland T, Fjeldbo CS, Lyng H. Tumor hypoxia as a barrier in cancer therapy: why levels matter. *Cancer*. 2021;13(3):499. doi:10.3390/cancers13030499
2. O'Connor JPB, Robinson SP, Waterton JC. Imaging tumour hypoxia with oxygen-enhanced MRI and BOLD MRI. *Br J Radiol*. 2019;92(1096):20180642. doi:10.1259/bjr.20180642
3. Bane O, Besa C, Wagner M, et al. Feasibility and reproducibility of BOLD and TOLD measurements in the liver with oxygen and carbogen gas challenge in healthy volunteers and patients with hepatocellular carcinoma. *J Magn Reson Imaging*. 2016;43(4):866-876. doi:10.1002/jmri.25051
4. Drew PJ, Chatterjee S, Turnbull LW, et al. Dynamic contrast enhanced magnetic resonance imaging of the breast is superior to triple assessment for the pre-operative detection of multifocal breast cancer. *Ann Surg Oncol*. 1999;6(6):599-603. doi:10.1007/s10434-999-0599-x
5. Colliez F, Gallez B, Jordan BF. Assessing tumor oxygenation for predicting outcome in radiation oncology: a review of studies correlating tumor hypoxic status and outcome in the preclinical and clinical settings. *Front Oncol*. 2017;7:10. doi:10.3389/fonc.2017.00010
6. Hallac RR, Zhou H, Pidikiti R, et al. Correlations of noninvasive BOLD and TOLD MRI with pO2 and relevance to tumor radiation response. *Magn Reson Med*. 2014;71(5):1863-1873. doi:10.1002/mrm.24846
7. Jiang L, Weatherall PT, McColl RW, Tripathy D, Mason RP. Blood oxygenation level-dependent (BOLD) contrast magnetic resonance imaging (MRI) for prediction of breast cancer chemotherapy response: a pilot study. *J Magn Reson Imaging*. 2013;37(5):1083-1092. doi:10.1002/jmri.23891
8. Hallac RR, Ding Y, Yuan Q, et al. Oxygenation in cervical cancer and normal uterine cervix assessed using blood oxygenation level-dependent (BOLD) MRI at 3T. *NMR Biomed*. 2012;25(12):1321-1330. doi:10.1002/nbm.2804

9. Burrell JS, Walker-Samuel S, Baker LC, et al. Exploring ΔR_2^* and ΔR_1 as imaging biomarkers of tumor oxygenation. *J Magn Reson Imaging*. 2013;38(2):429-434. doi:10.1002/jmri.23987
10. Guo Y, Jin N, Klein R, et al. Gas challenge-blood oxygen level-dependent (GC-BOLD) MRI in the rat Novikoff hepatoma model. *Magn Reson Imaging*. 2012;30(1):133-138. doi:10.1016/j.mri.2011.09.007
11. Remmele S, Sprinkart AM, Muller A, et al. Dynamic and simultaneous MR measurement of R1 and R2* changes during respiratory challenges for the assessment of blood and tissue oxygenation. *Magn Reson Med*. 2013;70(1):136-146. doi:10.1002/mrm.24458
12. Thomas CD, Chenu E, Walczak C, Plessis MJ, Perin F, Volk A. Morphological and carbogen-based functional MRI of a chemically induced liver tumor model in mice. *Magn Reson Med*. 2003;50(3):522-530. doi:10.1002/mrm.10555
13. Zhang K, Triphan SMF, Kurz FT, et al. Navigator-based slice tracking for prospective motion correction in kidney vessel architecture imaging. *Magn Reson Imaging*. 2023;98:26-35. doi:10.1016/j.mri.2023.01.001
14. Zhang K, Triphan SMF, Ziener CH, et al. Navigator-based slice tracking for kidney pCASL using spin-echo EPI acquisition. *Magn Reson Med*. 2023;90(1):231-239. doi:10.1002/mrm.29621
15. Zhang Z, Cho J, Wang L, et al. Blip up–down acquisition for spin- and gradient-echo imaging (BUDA-SAGE) with self-supervised denoising enables efficient T2, T2*, para- and dia-magnetic susceptibility mapping. *Magn Reson Med*. 2022;88(2):633-650. doi:10.1002/mrm.29219
16. Schmiedeskamp H, Straka M, Newbould RD, et al. Combined spin- and gradient-echo perfusion-weighted imaging. *Magn Reson Med*. 2012;68(1):30-40. doi:10.1002/mrm.23195
17. Schmiedeskamp H, Straka M, Bammer R. Compensation of slice profile mismatch in combined spin- and gradient-echo echo-planar imaging pulse sequences. *Magn Reson Med*. 2012;67(2):378-388. doi:10.1002/mrm.23012
18. Liu P, De Vis JB, Lu H. Cerebrovascular reactivity (CVR) MRI with CO2 challenge: a technical review. *NeuroImage*. 2019;187:104-115. doi:10.1016/j.neuroimage.2018.03.047
19. Cohen AD, Jagra AS, Visser NJ, et al. Improving the breath-holding CVR measurement using the multiband multi-echo EPI sequence. *Front Physiol*. 2021;12:619714. doi:10.3389/fphys.2021.619714
20. Kuppers F, Yun SD, Shah NJ. Development of a novel 10-echo multi-contrast sequence based on EPIK to deliver simultaneous quantification of T_2 and T_2^* with application to oxygen extraction fraction. *Magn Reson Med*. 2022;88(4):1608-1623. doi:10.1002/mrm.29305
21. Shen Y, Pu IM, Ahearn T, Clemence M, Schwarzbauer C. Quantification of venous vessel size in human brain in response to hypercapnia and hyperoxia using magnetic resonance imaging. *Magn Reson Med*. 2013;69(6):1541-1552. doi:10.1002/mrm.24258
22. Kritsaneepaiboon S, Ina N, Chotsampancharoen T, Roymanee S, Cheewatanakornkul S. The relationship between myocardial and hepatic T2 and T2*at 1.5T and 3T MRI in normal and iron-overloaded patients. *Acta Radiol*. 2018;59(3):355-362. doi:10.1177/0284185117715285
23. Meloni A, Carnevale A, Gaio P, et al. Liver T1 and T2 mapping in a large cohort of healthy subjects: normal ranges and correlation with age and sex. *Magn Reson Mater Phys Biol Med*. 2023;37(1):93-100. doi:10.1007/s10334-023-01135-6
24. Schwenzer NF, Machann J, Haap MM, et al. T2* relaxometry in liver, pancreas, and spleen in a healthy cohort of one hundred twenty-nine subjects-correlation with age, gender, and serum ferritin. *Invest Radiol*. 2008;43(12):854-860. doi:10.1097/RLI.0b013e3181862413
25. Ma J, Wehrli FW. Method for image-based measurement of the reversible and irreversible contribution to the transverse-relaxation rate. *J Magn Reson B*. 1996;111(1):61-69. doi:10.1006/jmrb.1996.0060
26. Zaitsev M, Akin B, LeVan P, Knowles BR. Prospective motion correction in functional MRI. *NeuroImage*. 2017;154:33-42. doi:10.1016/j.neuroimage.2016.11.014
27. Lee CC, Grimm RC, Manduca A, et al. A prospective approach to correct for inter-image head rotation in fMRI. *Magn Reson Med*. 1998;39(2):234-243. doi:10.1002/mrm.1910390210
28. Thesen S, Heid O, Mueller E, Schad LR. Prospective acquisition correction for head motion with image-based tracking for real-time fMRI. *Magn Reson Med*. 2000;44(3):457-465. doi:10.1002/1522-2594(200009)44:3%3C457::AID-MRM17%3E3.0.CO;2-R

SUPPORTING INFORMATION

Additional supporting information can be found online in the Supporting Information section at the end of this article.

How to cite this article: Zhang K, Triphan SMF, Wielpütz MO, et al. Navigator-based motion compensation for liver BOLD measurement with five-echo SAGE EPI and breath-hold task. *NMR in Biomedicine*. 2024;37(10):e5173. doi:10.1002/nbm.5173